Published on 19 May 2017. Downloaded by The University of Manchester Library on 30/11/2017 16:47:11.

Faraday Discussions

Cite this: *Faraday Discuss.*, 2017, **205**, 331

View Article Online
View Journal | View Issue

PAPER

Quantitative detection of isotopically enriched *E. coli* cells by SERS

Malama Chisanga,[a] Howbeer Muhamadali,[a] Richard Kimber[b] and Royston Goodacre *[a]

Received 27th April 2017, Accepted 19th May 2017
DOI: 10.1039/c7fd00150a

It is clear that investigating how bacterial cells work by analysing their functional roles in microbial communities is very important in environmental, clinical and industrial microbiology. The benefits of linking genes to their respective functions include the reliable identification of the causative agents of various diseases, which would permit appropriate and timely treatment in healthcare systems. In industrial and municipal wastewater treatment and management, such knowledge may allow for the manipulation of microbial communities, such as through bioaugmentation, in order to improve the efficiency and effectiveness of bioremediation processes. Stable isotope probing coupled with identification techniques has emerged to be a potentially reliable tool for the discrimination, identification and characterization of bacteria at community and single cell levels, knowledge which can be utilized to link microbially mediated bioprocesses to phylogeny. Development of the surface-enhanced Raman scattering (SERS) technique offers an exciting alternative to the Raman and Fourier-transform infrared spectroscopic techniques in understanding the metabolic processes of microorganisms *in situ*. SERS employing Ag and Au nanoparticles can significantly enhance the Raman signal, making it an exciting candidate for the analysis of the cellular components of microorganisms. In this study, *Escherichia coli* cells were cultivated in minimal medium containing different ratios of $^{12}C/^{13}C$ glucose and/or $^{14}N/^{15}N$ ammonium chloride as the only carbon and nitrogen sources respectively, with the overall final concentrations of these substrates being constant. After growth, the *E. coli* cells were analyzed with SERS employing an *in situ* synthesis of Ag nanoparticles. This novel investigation of the SERS spectral data with multivariate chemometrics demonstrated clear clusters which could be correlated to the SERS spectral shifts of biomolecules from cells grown and hence labelled with ^{13}C and ^{15}N atoms. These shifts reflect the isotopic content of the bacteria and quantification of the isotope levels could be established using chemometrics based on partial least squares regression.

[a]*School of Chemistry, Manchester Institute of Biotechnology, University of Manchester, Manchester, UK. E-mail: roy.goodacre@manchester.ac.uk; Tel: +44 (0) 161 306 4480*

[b]*School of Earth and Environmental Sciences, Williamson Research Centre for Molecular Environmental Science, University of Manchester, Manchester, UK*

Published on 19 May 2017. Downloaded by The University of Manchester Library on 30/11/2017 16:47:11.

Introduction

Bacteria and fungi very rarely live in isolation and are usually found in multi-species communities. In order to understand the roles of these organisms in complex environments a great deal of research has demonstrated the importance of linking specific microorganisms to their respective functional roles. These include: reliable identification of causative agents of various diseases which would permit appropriate and timely treatment in healthcare systems,[1] and within industrial and municipal wastewater treatment and management, such knowledge may allow for the manipulation of microbial communities, such as through bioaugmentation, in order to improve the efficiency and effectiveness of bioremediation processes.[2–4] Despite being admirable, these benefits remain largely unattainable, since whilst it is relatively easy to identify microorganisms within a community, there is considerable difficulty in linking organisms to their functional roles.[4,5]

The emergence of stable isotope probing (SIP) coupled with the development of genomics, transcriptomics and metabolomics techniques combined with advanced identification technologies has recently started to bridge this gene (organism) to function gap.[6,7] Ideally, the SIP approach involves the incorporation of heavy isotopes, *via* the metabolism of a labelled substrate, into bacterial components such as polar-lipid-derived fatty acids (PLFAs), proteins, DNA, metabolites *etc.*, allowing for direct identification of the 'victim' bacterium or group of bacteria that have preferentially used a labelled substrate.[8,9] Several studies have demonstrated the utility of SIP for linking the taxonomic identity (*via* 16S rDNA) of bacteria to function, which mainly focused on the analysis and discrimination of isotopically enriched PLFA,[10–12] DNA[8,13,14] and RNA.[4,15–17] However, the difficulties involved in resolving PLFA signatures of multi-species components as well as the limitation of isotopic enrichment due to the need of having a significant amount of labelled DNA that can be separated by isotope gradient-based centrifugation may limit the global use of PLFA and DNA-based SIP strategies.[7,18] Recently, Raman spectroscopy combined with SIP has attracted a lot of attention as a tool for linking gene to function.[19–21] As opposed to PLFA, DNA and RNA, Raman-based SIP permits rapid, non-destructive and high throughput identification and discrimination of the bacteria responsible for metabolising labelled substrates at community and, more importantly, single cell levels.[19,22] In Raman scattering, the differentiation of labelled and unlabelled bacteria is based on respective 'redshifts' (vibrations that move to lower wavenumber shifts) of the Raman spectral peaks arising from specific molecular vibrations of polarizable chemical bonds in labelled biomolecules such as carbohydrates, proteins, nucleic acids and lipids.[23] Therefore, Raman-based SIP may reveal a vast amount of information regarding the heterogeneity, cell–cell interactions, structural properties and physiological dynamics of bacteria in their natural populations.[20,24] In spite of this Raman-SIP approach being applied in medical,[25,26] food,[27] and environmental[28] areas, Raman spectroscopy is held back by its naturally poor quantum efficiency: only $\sim$1 in 10^6 to 10^8 incident photons undergo inelastic scattering. This limits the sensitivity of Raman techniques which may lead to long acquisition times. Consequently, this prevents Raman techniques from being applied in routine clinical and industrial laboratories.[29]

 This journal is © The Royal Society of Chemistry 2017

Published on 19 May 2017. Downloaded by The University of Manchester Library on 30/11/2017 16:47:11.

Surface-enhanced Raman scattering (SERS) has been developed in order to improve the sensitivity and the Raman signal (typically by 10^3 to 10^6 times).[30] Strong SERS signals originate from biomolecules in close proximity to, or adsorbed on to, carefully prepared nanometre-sized Ag or Au particles, roughened metal surfaces or thin films.[31] Kubryk and colleagues reported the first application of SERS for single cell analysis.[32] Interestingly, the same technique was employed for determining the biomolecules responsible for the major SERS spectral band around 730 cm^{-1}.[33] Nevertheless, SERS is limited by the lack of reproducibility due to a number of factors including the heterogeneity of the nanoparticle sizes and poor bacteria-nanoparticle interactions.[34] However, recent studies have demonstrated that by optimizing the nanoparticle synthesis process and through careful design of the experimental parameters, highly reproducible SERS spectra can be achieved.[35–39]

In this study, for the first time, we illustrate the quantitative differentiation of bacteria labelled with varying concentrations of $^{12}C/^{13}C$-glucose and/or $^{14}N/^{15}N$-ammonium chloride using SERS involving an *in situ* synthesis of silver nanoparticles,[40] along with multivariate chemometrics of the resultant SERS spectra.

Experimental methods

Growth conditions

Unless otherwise stated, all chemicals were purchased from Fisher (Fisher Scientific, UK).

Escherichia coli K-12 MG1655 was grown on minimal medium supplemented with 5 g L^{-1} of varying concentrations of ^{12}C-glucose and/or 99 atom% homogeneously labelled ^{13}C-glucose (both purchased from Sigma Aldrich, UK), and 1 g L^{-1} of varying ratios of ^{14}N–NH_4Cl and/or 98 atom% homogeneously labelled ^{15}N–NH_4Cl (Sigma Aldrich, UK), as the single carbon and nitrogen sources respectively.[22] Bacterial samples were incubated as 1.5 mL aliquot replicates ($n = 5$) in sterile 24-well plates (Greiner Bio-one, UK) for 15 h at 37 °C with a 170 rpm shaking speed in a Multitron standard shaker incubator (INFORS-HT Bottmingen, Switzerland). To reduce the potential evaporation and loss of sample during the incubation period, all plates were sealed with sterile Breathe-Easy sealing membranes (Sigma Aldrich, UK). All the cells were harvested at the stationary growth phase ($t = 15$ h) for SERS measurements.

Sample preparation

After incubation, each sample aliquot (1.5 mL) was transferred to a sterile 2 mL microcentrifuge tube and centrifuged for 5 min at 5000*g* using a bench top Eppendorf Microcentrifuge 5424R (Eppendorf Ltd, Cambridge, UK). After discarding the supernatant, the collected biomass was washed twice using 1 mL of de-ionized water to remove the media components following the above centrifugation. The pellets were collected and stored at −80 °C prior to SERS analysis.

In situ synthesis of colloidal silver nanoparticles

The preparation of the sodium borohydride-reduced silver nanoparticles described in this study follows Zeiri,[40] Efrima[35] and the method described by Lee

Published on 19 May 2017. Downloaded by The University of Manchester Library on 30/11/2017 16:47:11.

and Meisel[41] with small modifications. Briefly, the bacterial pellets were suspended in 0.09 M sodium borohydride solution and centrifuged for 10 min at 2800 *g*. After removing the supernatant, the pellets were resuspended in 0.04 M silver nitrate solution; at this point the silver cations were reduced by the borohydride anions to form Ag nanoparticles which were adsorbed onto the surface of the intact bacterial cells as shown by the schematic diagram in Fig. 1a and in the SEM image in Fig. 1c.[35,38]

Raman microspectroscopy analysis

Prior to the Raman measurements, 5 μL of each of the bacteria-silver nanoparticle solutions were spotted onto clean and dry calcium fluoride (CaF_2) discs and air-dried for 30 min in a desiccator. SERS spectra were obtained as mapping scans using an InVia confocal Raman spectrometer (Renishaw Plc., Gloucestershire, UK) equipped with a 532 nm diode laser with the laser power on the sample adjusted to 0.024 mW. The wavelength of the instrument was calibrated with a silicon wafer focused under the 50× objective and collected as a static spectrum centered at 520 cm^{-1}. The experimental parameters were maintained throughout

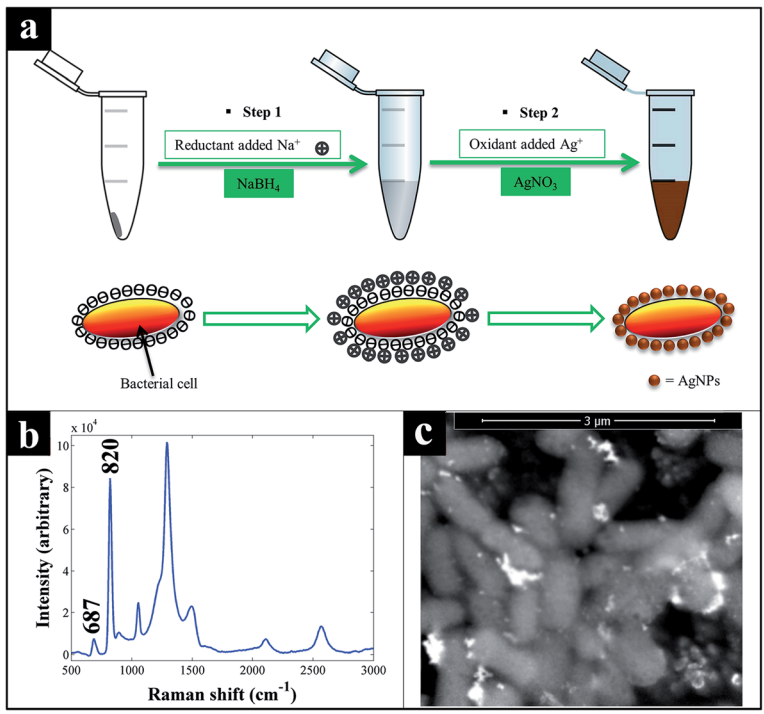

Fig. 1 (a) Schematic illustration of the steps employed in this experiment leading to the formation of Ag nanoparticles. The silver cations are reduced by the borohydride reducing agent resulting in the formation of Ag nanoparticles which adsorb onto the *E. coli* cell surfaces; (b) SERS spectrum of the Ag nanoparticles obtained using the same instrumental parameters as for all samples. The peaks at 687 and 820 cm^{-1} are clearly linked with the Ag nanoparticles and not the samples; (c) SEM image of a thin film of intact *E. coli* cells coated with sodium borohydride-reduced Ag nanoparticles.

Published on 19 May 2017. Downloaded by The University of Manchester Library on 30/11/2017 16:47:11.

the analysis as: 25 s exposure time, 8 accumulations and 600 L mm^{-1} grating, with each spectrum collected from 500 to 3000 cm^{-1}.

SERS imaging was undertaken using the same instrument and laser wavelength as mentioned above. The spectral data were collected from 500 to 3000 cm^{-1} using a streamline mode with a 60 s exposure time, 1 accumulation and 1 μm step size.

Scanning electron microscopy (SEM) analysis

After the bacteria-nanoparticle samples were washed and resuspended in deionized water, 100 μL of the sample was spotted onto a clean carbon pad supported on an aluminum stub and allowed to dry. SEM images (Fig. 1c) were taken using an FEI Quanta 650 ESEM-FEG operating under high vacuum with an accelerating voltage of 10 kV.

Data analysis

All statistical analysis was carried out with MATLAB version 2015a (The MathWorks Inc., Natwick, US). All the collected SERS spectra were baseline corrected using asymmetric least squares (AsLS),[42] and scaled by applying the extended multiplicative signal correction (EMSC) method.[43] The unsupervised method of principal component analysis (PCA) was employed to reduce the dimensionality of the data, followed by discriminant function analysis (PC-DFA).[44,45] PC-DFA functions by minimising within class variance and simultaneously maximising between class variance. The first 20 PCs with a total explained variance (TEV) of 95.9% were used to generate the PC-DFA model, the class structures used were the technical repeats and so this approach is considered as only semi-supervised; *i.e.* the algorithm is not told the amount of isotope to which the bacteria had been cultivated in.

To effect quantitative analysis, partial least square regression (PLSR)[46] was employed to predict the concentrations of $^{12}C/^{13}C$ and $^{14}N/^{15}N$ using the entire SERS spectral data from 500 to 3000 cm^{-1}.

PCA was also applied to the SERS image to visualize the contrast in the image according to the PC scores. The PCA loadings were subsequently inspected to identify the significant peaks contributing to such contrast.

Results and discussion

The SERS-based SIP technique is emerging as a powerful and valuable platform for the identification, differentiation, discrimination and characterization of microorganisms associated with particular vital functions in complex microbial communities.[32] Nevertheless, the studies reported so far are generally focused on cultivating bacteria in fully labelled substrates or partially labelled ^{13}C-glucose only to reveal useful information about the metabolic capabilities of microorganisms.[32,33] Thus, the aim of our study is to demonstrate the potential application of SERS-based SIP as a metabolic fingerprinting platform for the quantitative detection and differentiation of *E. coli* cells grown on different ratios of isotopically enriched ^{13}C-glucose and/or ^{15}N-ammonium chloride substrates. The total concentration of these substrates was kept constant at 5 g L^{-1} glucose and 1 g L^{-1} nitrogen, and it is perhaps worth noting

Published on 19 May 2017. Downloaded by The University of Manchester Library on 30/11/2017 16:47:11.

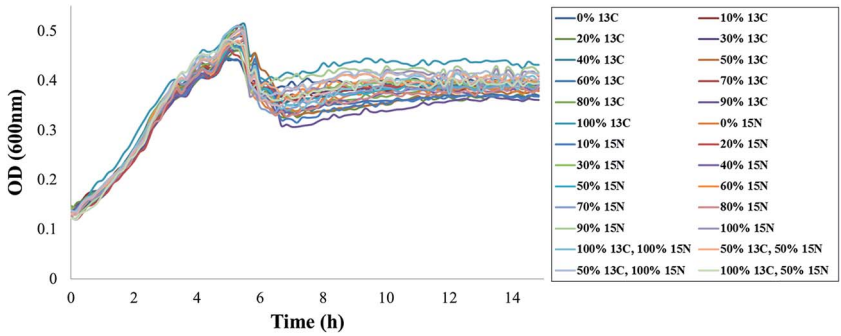

Fig. 2 Growth curves of the *E. coli* cells labelled with different ratios of ^{13}C and/or ^{15}N.

that although the *E. coli* cells were exposed to different ratios of isotopically labelled carbon and nitrogen substrates in this experiment, the growth profiles (Fig. 2) of the cells were comparable and not affected by the varying concentrations of the heavy isotopes, which is also consistent with our previously reported findings.[22] This means that all of the *E. coli* cells were phenotypically identical, and any quantitative differences which were seen in the SERS spectra of these cells would be entirely attributed to the varying isotopic content of the cells as a function of their metabolic activity.

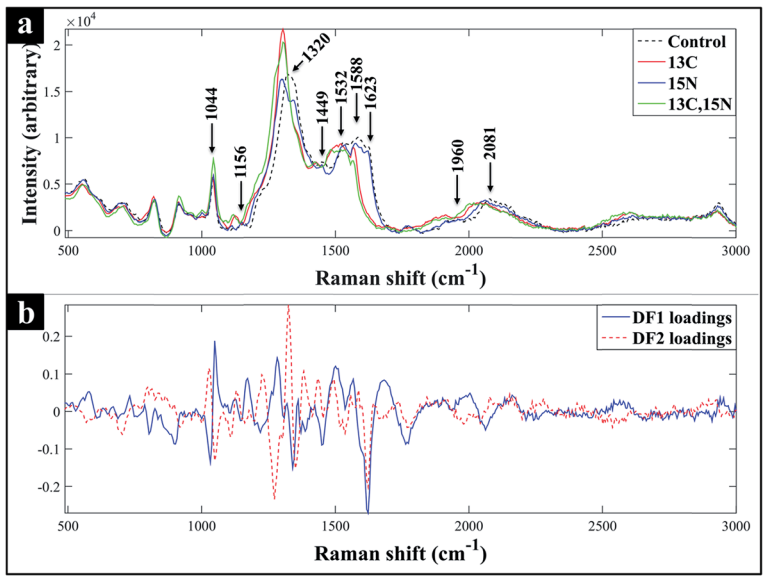

Fig. 3 (a) SERS spectra of the *E. coli* cells cultivated on unlabelled substrates (black dotted line), ^{13}C labelled (red line), ^{15}N labelled (blue line), and ^{13}C and ^{15}N labelled (green line) cells are also shown where cells were cultivated in either 0% or 100% ^{13}C-glucose and ^{15}N-ammonium chloride as the only source of carbon and nitrogen, and (b) PC-DFA loadings plot of the SERS spectral data with DF1 (blue line) and DF2 (red line) showing the major peaks affected by the labelling process. The DFA loadings plot corresponds to the DFA scores plot shown in Fig. 4.

 This journal is © The Royal Society of Chemistry 2017

Published on 19 May 2017. Downloaded by The University of Manchester Library on 30/11/2017 16:47:11.

SERS metabolic fingerprints

Fig. 3a displays the average SERS spectra of the *E. coli* cells cultivated on normal (^{12}C and ^{14}N) and isotopically labelled (^{13}C and ^{15}N) substrates for 15 h. These spectra display clear shifts of various bands to lower wavenumbers (so called 'redshift') due to the increase in the reduced mass which leads to a decrease in the vibrational frequencies (wavenumbers) of chemical bonds when ^{13}C and ^{15}N 'heavy' isotopes are incorporated.[47] Details of the affected bands and their corresponding vibrational assignments are provided in Table 1. By visual inspection, the major spectral bands affected by ^{13}C incorporation are at 2081, 1623, 1532 and 1449 cm^{-1} which are tentatively assigned to C–N stretching, olefinic C=C stretching, C–H bending or C=C stretching, and CH_2 scissoring vibrations respectively.

As one may have predicted, when the cells are subjected to ^{15}N atoms the bands at 2081 and 1320 cm^{-1}, tentatively ascribed to the C–N stretching, C–N ring and NH_2 stretching vibrations respectively, are those that are mainly affected. The SERS bands at 1960, 1623, 1532 and 1449 cm^{-1} do not show any significant shifts upon exposure to ^{15}N atoms, suggesting that the nitrogen atom does not contribute to these vibrational modes. The unique band which emerges at 1341 cm^{-1} upon ^{15}N incorporation may be assigned to the isotopologues of nitrogen containing compounds such as adenine. Interestingly, when the cells are grown on both ^{13}C and ^{15}N atoms, the bands at 2081, 1588, 1320 and 1156 cm^{-1} display further shifts (by 63, 72, 48 and 37 (Δ cm^{-1}) respectively) illustrating the joint contributions of both ^{13}C and ^{15}N atoms to the vibrational modes. These vibrations are likely to be derived from biomolecules such as proteins, DNA and amides that possess C–N chemical bonds in their molecular structures.

It is also clear that the SERS spectral bands in Fig. 3a are dominated by vibrations linked to carbon atoms either linked to another carbon or to a nitrogen atom. According to previous reports, these vibrational modes are probably derived predominantly from adenine[48] and adenine derivatives such

Table 1 Tentative band assignments for SERS spectra

Unlabelled cells (cm^{-1})	Only ^{13}C-labelled (Δ cm^{-1})	Only ^{15}N-labelled (Δ cm^{-1})	Dual ^{13}C, ^{15}N-labelled (Δ cm^{-1})	Tentative band assignment[a]
2081	−39	−24	−63	C–N stretch, adenine, FAD, NAG
1960	−49	0	−49	C=C stretch
1623	−56	0	−61	C=C stretch, olefinic
1588	−67	−10	−72	C–N stretch, proteins, DNA, amides
1532	−11	0	−11	C–H bend or C=C stretch
1449	−25	0	−25	CH_2 scissor
1320	−16	−27	−48	C–N, N–H stretch, adenine, DNA
1156	−32	−5	−37	C–N stretch, amides, DNA, adenine
1044	0	0	0	O–P–O stretch in the phosphate group, FAD

[a] FAD, flavin adenine dinucleotide; NAG, *N*-acetyl glucosamine.

Published on 19 May 2017. Downloaded by The University of Manchester Library on 30/11/2017 16:47:11.

as hypoxanthine (product of purine degradation), flavin adenine dinucleotide (FAD),[33,40] *N*-acetyl glucosamine (NAG) and other components of peptidoglycan,[31,37,49] as well as adenosine triphosphate (ATP).[40,50,51] Several bands in the fingerprint region do not move no matter what the level of isotope incorporation is; for example, the band at 1044 cm^{-1} may be due to a phosphate vibrational mode from molecules such as flavin adenine dinucleotide (FAD). Since the cells were still intact after the *in situ* synthesis of Ag nanoparticles as shown in Fig. 1c, the SERS spectral features are believed to have emerged from the vibrational modes of the biomolecules present in the cell wall of the *E. coli* bacteria. Finally, the Ag nanoparticle peaks at 687 and 820 cm^{-1} as illustrated in the spectrum of the Ag colloid only (Fig. 1b) are also unaffected by any isotopic labelling. As these were consistent, they confirm that the shifts observed are due to the incorporation of the heavy isotopes by the cells and are not an artefact of sample to sample variation or instrument drift.

All pre-processed SERS spectral data (AsLS followed by EMSC) were subjected to PC-DFA to investigate any natural clustering patterns resulting from ^{13}C and/or ^{15}N incorporation by *E. coli* cells, as well as to assess the reproducibility of the spectral data. The PC-DFA scores plot of all the data (Fig. 4) revealed a clear separation between the spectra of the *E. coli* cells incorporated with $^{12}C/^{13}C$, $^{14}N/^{15}N$ and those with different combinations of both ^{13}C and ^{15}N according to the concentration and ratio of the isotopic content. As can be seen in Fig. 4, the first discriminant function (DF1) reflects the increasing ratio of ^{13}C in bacterial cells from left to right, which also confirms that the carbon-related vibrations dominated the SERS spectral data. In addition, bacteria with an increasing ^{15}N ratio are separated from top to bottom along the DF2 axis

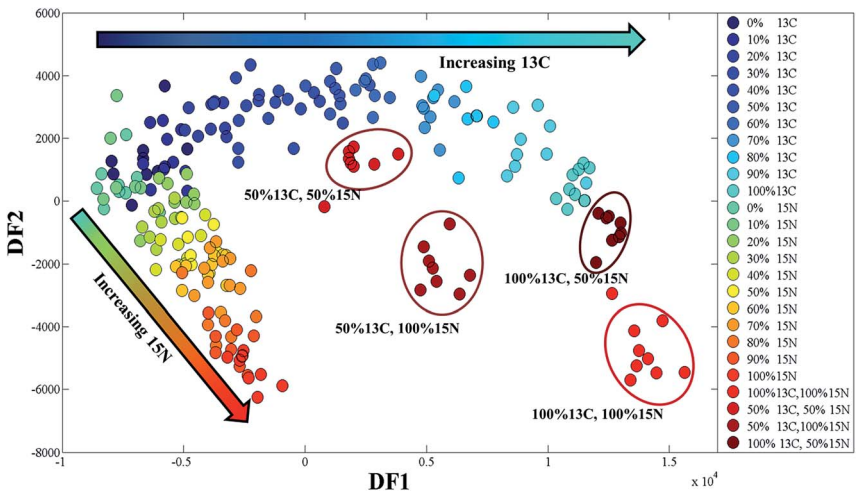

Fig. 4 PC-DFA scores plot of the pre-processed SERS spectral data of *E. coli* cells cultivated on different ratios of unlabelled (^{12}C and ^{14}N) and isotopically labelled ^{13}C and/or ^{15}N growth substrates. The arrows indicate increments in the ratios of the labelled substrates. Elipses are used to highlight the cells grown on mixtures of ^{13}C and ^{15}N, and have no statistical relevance.

Published on 19 May 2017. Downloaded by The University of Manchester Library on 30/11/2017 16:47:11.

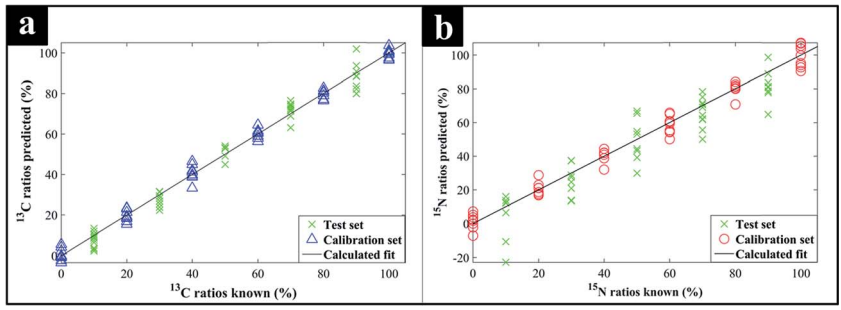

Fig. 5 PLSR models of the SERS spectra generated for a quantitative prediction of the ^{13}C (a) and ^{15}N (b) ratios in the test sets. The calibration and test sets are represented by green crosses and blue triangles respectively. The statistics associated with these models are presented in Table 2.

(Fig. 4), while cells containing combinations of both the heavy isotopes are also clustered where one would expect as they contain contributions from both ^{13}C as well as ^{15}N. The PC-DFA loadings plot (Fig. 3b) displays the most significant vibrations contributing to the observed clustering patterns, which is also in agreement with the wavenumber shifts identified by visual inspection of the spectra (Fig. 3a). These bands have been discussed above and are reported in Table 1.

The next stage of the analysis was to establish further the level of quantitative information that could be extracted from the SERS spectra from bacteria labelled with different levels of ^{13}C or ^{15}N. PLSR was employed to generate two models for each isotope (^{13}C, ^{15}N). The predictions for the PLSR models are shown in Fig. 5 and it is clear that there is abundant information in the SERS spectra that allows for excellent predictions of the amount of ^{13}C-glucose and ^{15}N–NH_4Cl that the *E. coli* were cultivated in. A very low root mean square error of cross validation (RMSECV from the calibration/training data) and the root mean square error of prediction (RMSEP from the test set) confirm the high prediction accuracy (Table 2). Moreover, the fact that R^2 and Q^2 are close to one illustrates the excellent linearity of the predictions. We do note that the PLSR model of the ^{13}C data displayed higher accuracy and reproducibility and this could again be due to the higher abundance of carbon related vibrations in the spectra.

Table 2 Statistics on the PLSR models on the SERS data to illustrate the reproducibility and accuracy for predicting the ratios of the isotopic labels[a]

Isotope	Factors	Q^2	R^2	RMSEP	RMSECV
^{13}C	5	0.9738	0.9940	4.7203	5.3380
^{15}N	5	0.8161	0.9814	11.7475	8.7609

[a] Where: correlation of predictions to known isotope levels for the test set (Q^2) and calibration/training set (R^2); RMSEP, root mean squared error of prediction from the test set; RMSECV, root mean squared error of cross validation from the calibration/training data.

Published on 19 May 2017. Downloaded by The University of Manchester Library on 30/11/2017 16:47:11.

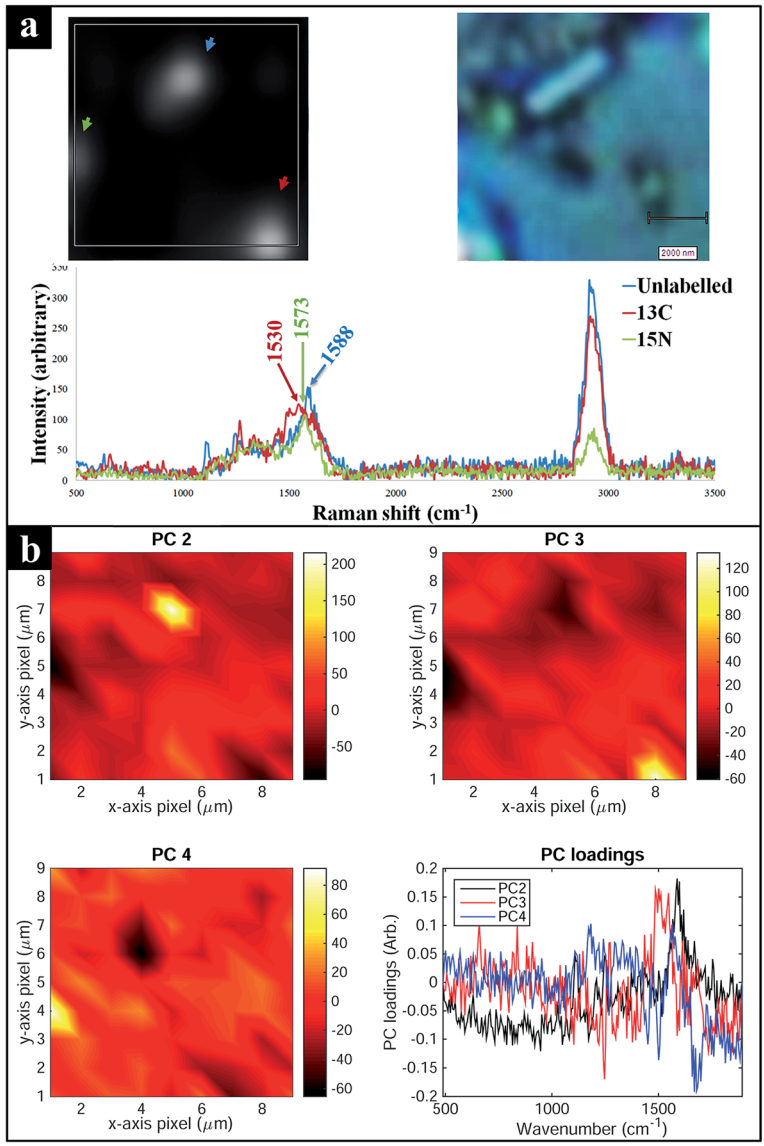

Fig. 6 SERS images of isotopically labelled intact single *E. coli* cells. (a) SERS and a corresponding white light image of three single *E. coli* cells, and the representative spectra of each single bacterium (indicated by the arrows). The grey shading represents the peak intensity at 1588 cm^{-1}. (b) PCA scores and image reconstruction of the SERS spectral data collected between 500–1800 cm^{-1}, and their corresponding loadings plot; the first PC score is not shown as this only differentiates between the bacterial biomass and CaF_2 background.

Conclusions

This study demonstrates a novel application of SERS combined with isotopic labelling for the quantitative detection and differentiation of *E. coli* cells, even though the cells are phenotypically identical. When incorporated with varying ratios of labelled ^{13}C and/or ^{15}N isotopes, the SERS spectral bands displayed clear

Published on 19 May 2017. Downloaded by The University of Manchester Library on 30/11/2017 16:47:11.

redshifts that were used as the basis for quantitative characterization of bacteria at the molecular level. The observed shifts in the SERS spectral data were also evident in the PC-DFA loadings plots and the PLSR models clearly illustrate the highly quantitative nature of the SERS metabolic fingerprints. In addition, we have illustrated for the first time that highly reproducible SERS of bacteria cultivated on different combinations of ^{13}C and ^{15}N can be achieved using an *in situ* synthesis of borohydride-reduced Ag nanoparticles. The findings of this study also highlight the importance of the choice of protocols (*e.g.* microbial sample preparation and nanoparticle synthesis) and instruments (laser wavelength) used for the bacterial SERS analysis, which may consequently reveal or suppress specific spectral features. For example, Kubryk and colleagues used hydroxylammonium chloride solution as the reduction agent and employed a 633 nm laser to acquire SERS spectra of isotopically labelled bacterial cells. These authors reported major shifts occurring at 733 and 1330 cm^{-1}, whilst in this study using sodium borohydride as the reduction agent and a 532 nm laser, the peak at 733 cm^{-1} was not detected. However, by contrast in this study and as a consequence of using different protocols, various other peaks were detected (such as: 2081, 1960, 1623, 1588 and 1532 cm^{-1}) which displayed clear shifts upon isotopic substitution and the PC-DFA and PLSR analyses showed that these contributed to the quantification process. Whilst our approach does indicate that there are more bands that are isotopically labelled compared to the study carried out by Kubryk and coworkers, we do agree with these authors that stable isotopes can be highly beneficial in assigning peaks to the specific vibrational modes of compounds, as illustrated in Table 1 for assigning vibrations that contain either ^{13}C or ^{15}N or both heavy isotopes. In this study we have illustrated this with ^{13}C and ^{15}N, and would expect that such an approach would work with other stable isotopes such as ^{18}O and ^{34}S, as well as other instable isotopes (*e.g.* ^{33}P), from atoms which are routinely found in metabolites and proteins within bacterial and indeed eukaryotic cells.

One would expect these SERS band shifts to be diagnostically useful as their precise initial positions (from natural isotopes) are a consequence of natural metabolites and protein differences in the bacterial cell. We have shown previously that SERS of bacteria can allow for the identification of bacteria that are of clinical and industrial relevance[52] down to sub-species levels.[31] Thus when SERS is augmented by isotope labelling, SIP-SERS will give information on both the function of the organism as well as its differentiation within complex communities.

We believe that SERS-based SIP combined with multivariate chemometrics presents an exciting avenue with a huge potential for application in the assignment of taxonomic identities to microbially driven bioprocesses in complex microbial communities, which will aid in linking gene to function. To illustrate this, Fig. 6a shows SERS images (with a pixel resolution of 1 μm under a built-in normal light microscope with a voxel diameter and volume of <1 μm (equivalent to the average size of an *E. coli* cell) and ~1 pL respectively) where it is clear that bacterial cells that are labelled with heavy isotopes can be readily differentiated from bacteria grown on natural isotope containing substrates. This is also evident from the PCA scores (Fig. 6b) where unlabelled, ^{13}C labelled and ^{15}N labelled *E. coli* cells can be clearly differentiated using PC2, PC3 and PC4 respectively. It is also worth noting that the affected peaks (1588 cm^{-1}, C–N stretching) identified using the loadings plots (Fig. 6b) are in complete agreement with the corresponding SERS spectra (Fig. 6a).

Published on 19 May 2017. Downloaded by The University of Manchester Library on 30/11/2017 16:47:11.

Acknowledgements

MC is funded by the Commonwealth Scholarship Commission, UK. HM and RG thank the European Commission's Seventh Framework Program for funding (STREPSYNTH; Project No. 613877). RG is indebted to UK BBSRC (BB/L014823/1) for funding for Raman spectroscopy. We would like to thank Professor Jonathan Lloyd for assisting us with the ESEM instrument.

References

1 L. N. Slater, D. F. Welch, D. Hensel and D. W. Coody, *N. Engl. J. Med.*, 1990, **323**, 1587–1593.
2 K. Watanabe, M. Teramoto, H. Futamata and S. Harayama, *Appl. Environ. Microbiol.*, 1998, **64**, 4396–4402.
3 R. Madsen, T. Lundstedt and J. Trygg, *Anal. Chim. Acta*, 2010, **659**, 23–33.
4 M. Manefield, A. S. Whiteley, R. I. Griffiths and M. J. Bailey, *Appl. Environ. Microbiol.*, 2002, **68**, 5367–5373.
5 R. I. Amann, W. Ludwig and K. H. Schleifer, *Microbiol. Rev.*, 1995, **59**, 143–169.
6 M. G. Dumont and J. C. Murrell, *Nat. Rev. Microbiol.*, 2005, **3**, 499–504.
7 J. D. Neufeld, M. G. Dumont, J. Vohra and J. C. Murrell, *Microb. Ecol.*, 2007, **53**, 435–442.
8 S. Radajewski, P. Ineson, N. R. Parekh and J. C. Murrell, *Nature*, 2000, **403**, 646–649.
9 S. Behrens, T. Losekann, J. Pett-Ridge, P. K. Weber, W. O. Ng, B. S. Stevenson, I. D. Hutcheon, D. A. Relman and A. M. Spormann, *Appl. Environ. Microbiol.*, 2008, **74**, 3143–3150.
10 H. T. S. Boschker, S. C. Nold, P. Wellsbury, D. Bos, W. de Graaf, R. Pel, R. J. Parkes and T. E. Cappenberg, *Nature*, 1998, **392**, 801–805.
11 P. Roslev and N. Iversen, *Appl. Environ. Microbiol.*, 1999, **65**, 4064–4070.
12 Y. Chen, M. G. Dumont, N. P. McNamara, P. M. Chamberlain, L. Bodrossy, N. Stralis-Pavese and J. C. Murrell, *Environ. Microbiol.*, 2008, **10**, 446–459.
13 G. Webster, L. C. Watt, J. Rinna, J. C. Fry, R. P. Evershed, R. J. Parkes and A. J. Weightman, *Environ. Microbiol.*, 2006, **8**, 1575–1589.
14 M. W. Friedrich, *Curr. Opin. Biotechnol.*, 2006, **17**, 59–66.
15 M. P. Ginige, P. Hugenholtz, H. Daims, M. Wagner, J. Keller and L. L. Blackall, *Appl. Environ. Microbiol.*, 2004, **70**, 588–596.
16 A. S. Whiteley, M. Manefield and T. Lueders, *Curr. Opin. Biotechnol.*, 2006, **17**, 67–71.
17 Y. Kasai, Y. Takahata, M. Manefield and K. Watanabe, *Appl. Environ. Microbiol.*, 2006, **72**, 3586–3592.
18 R. E. Drenovsky, K. P. Feris, K. M. Batten and K. Hristova, *Am. Midl. Nat.*, 2008, **160**, 140–159.
19 W. E. Huang, R. I. Griffiths, I. P. Thompson, M. J. Bailey and A. S. Whiteley, *Anal. Chem.*, 2004, **76**, 4452–4458.
20 Y. Wang, Y. T. Ji, E. S. Wharfe, R. S. Meadows, P. March, R. Goodacre, J. Xu and W. E. Huang, *Anal. Chem.*, 2013, **85**, 10697–10701.
21 Y. Wang, W. E. Huang, L. Cui and M. Wagner, *Curr. Opin. Biotechnol.*, 2016, **41**, 34–42.
22 H. Muhamadali, M. Chisanga, A. Subaihi and R. Goodacre, *Anal. Chem.*, 2015, **87**, 4578–4586.

 This journal is © The Royal Society of Chemistry 2017

Published on 19 May 2017. Downloaded by The University of Manchester Library on 30/11/2017 16:47:11.

23 W. E. Huang, M. Q. Li, R. M. Jarvis, R. Goodacre and S. A. Banwart, in *Advances in Applied Microbiology*, ed. A. I. Laskin, S. Sariaslani and G. M. Gadd, Elsevier Academic Press Inc, San Diego, 2010, vol. 70, pp. 153–186.
24 Y. Wang, Y. Z. Song, Y. F. Tao, H. Muhamadali, R. Goodacre, N. Y. Zhou, G. M. Preston, J. Xu and W. E. Huang, *Anal. Chem.*, 2016, **88**, 9443–9450.
25 K. Maquelin, C. Kirschner, L. P. Choo-Smith, N. van den Braak, H. P. Endtz, D. Naumann and G. J. Puppels, *J. Microbiol. Methods*, 2002, **51**, 255–271.
26 R. Goodacre, E. M. Timmins, R. Burton, N. Kaderbhai, A. M. Woodward, D. B. Kell and P. J. Rooney, *Microbiology*, 1998, **144**, 1157–1170.
27 N. Nicolaou, Y. Xu and R. Goodacre, *Anal. Chem.*, 2011, **83**, 5681–5687.
28 S. A. Eichorst, F. Strasser, T. Woyke, A. Schintlmeister, M. Wagner and D. Woebken, *FEMS Microbiol. Ecol.*, 2015, **91**, 1–14.
29 L. Ashton, K. Lau, C. L. Winder and R. Goodacre, *Future Microbiol.*, 2011, **6**, 991–997.
30 M. Kahraman, M. M. Yazici, F. Sahin, O. F. Bayrak and M. Culha, *Appl. Spectrosc.*, 2007, **61**, 479–485.
31 R. M. Jarvis and R. Goodacre, *Anal. Chem.*, 2004, **76**, 40–47.
32 P. Kubryk, J. S. Kolschbach, S. Marozava, T. Lueders, R. U. Meckenstock, R. Niessner and N. P. Ivleva, *Anal. Chem.*, 2015, **87**, 6622–6630.
33 P. Kubryk, R. Niessner and N. P. Ivleva, *Analyst*, 2016, **141**, 2874–2878.
34 H. Fisk, C. Westley, N. J. Turner and R. Goodacre, *J. Raman Spectrosc.*, 2016, **47**, 59–66.
35 S. Efrima and L. Zeiri, *J. Raman Spectrosc.*, 2009, **40**, 277–288.
36 M. Kahraman, M. M. Yazici, F. Sahin and M. Culha, *J. Biomed. Opt.*, 2007, **12**, 1–6.
37 R. M. Jarvis, A. Brooker and R. Goodacre, *Faraday Discuss.*, 2006, **132**, 281–292.
38 R. M. Jarvis, A. Brooker and R. Goodacre, *Anal. Chem.*, 2004, **76**, 5198–5202.
39 M. Moskovits, *J. Raman Spectrosc.*, 2005, **36**, 485–496.
40 L. Zeiri, B. V. Bronk, Y. Shabtai, J. Czege and S. Efrima, *Colloids Surf., A*, 2002, **208**, 357–362.
41 P. C. Lee and D. Meisel, *J. Phys. Chem.*, 1982, **86**, 3391–3395.
42 P. H. C. Eilers, *Anal. Chem.*, 2004, **76**, 404–411.
43 H. Martens, J. P. Nielsen and S. B. Engelsen, *Anal. Chem.*, 2003, **75**, 394–404.
44 H. J. H. Macfie, C. S. Gutteridge and J. R. Norris, *J. Gen. Microbiol.*, 1978, **104**, 67–74.
45 P. S. Gromski, H. Muhamadali, D. I. Ellis, Y. Xu, E. Correa, M. L. Turner and R. Goodacre, *Anal. Chim. Acta*, 2015, **879**, 10–23.
46 P. Geladi and B. R. Kowalski, *Anal. Chim. Acta*, 1986, **185**, 1–17.
47 P. J. Larkin, *Infrared and Raman Spectroscopy: Principles and Spectral Interpretation*, Elsevier Science Bv, Amsterdam, 2011.
48 W. R. Premasiri, Y. Gebregziabher and L. D. Ziegler, *Appl. Spectrosc.*, 2011, **65**, 493–499.
49 T. T. Liu, Y. H. Lin, C. S. Hung, T. J. Liu, Y. Chen, Y. C. Huang, T. H. Tsai, H. H. Wang, D. W. Wang, J. K. Wang, Y. L. Wang and C. H. Lin, *PLoS One*, 2009, **4**, 1–10.
50 A. Walter, A. Marz, W. Schumacher, P. Rosch and J. Popp, *Lab Chip*, 2011, **11**, 1013–1021.
51 M. Kahraman, M. M. Yazici, F. Sahin, O. F. Bayrak, E. Topcu and M. Culha, *Int. J. Environ. Anal. Chem.*, 2007, **87**, 763–770.
52 H. Muhamadali, A. Subaihi, M. Mohammadtaheri, Y. Xu, D. I. Ellis, R. Ramanathan, V. Bansal and R. Goodacre, *Analyst*, 2016, **141**, 5127–5136.